Taylor & Francis
Taylor & Francis Group

Journal of Macromolecular Science, Part A
Pure and Applied Chemistry

ISSN: 1060-1325 (Print) 1520-5738 (Online) Journal homepage: https://www.tandfonline.com/loi/lmsa20

Photocatalytic activities of poly(methyl methacrylate)/titanium dioxide nanofiber mat

Ozcan Koysuren & H. Nagehan Koysuren

To cite this article: Ozcan Koysuren & H. Nagehan Koysuren (2017) Photocatalytic activities of poly(methyl methacrylate)/titanium dioxide nanofiber mat, Journal of Macromolecular Science, Part A, 54:2, 80-84, DOI: 10.1080/10601325.2017.1261619

To link to this article: https://doi.org/10.1080/10601325.2017.1261619

JOURNAL OF MACROMOLECULAR SCIENCE, PART A: PURE AND APPLIED CHEMISTRY
2017, VOL. 54, NO. 2, 80–84
http://dx.doi.org/10.1080/10601325.2017.1261619

Taylor & Francis
Taylor & Francis Group

Photocatalytic activities of poly(methyl methacrylate)/titanium dioxide nanofiber mat

Ozcan Koysuren[a] and H. Nagehan Koysuren[b]

[a]Department of Energy and Materials Engineering, Ankara University, Ankara, Turkey; [b]Department of Environmental Engineering, Ahi Evran University, Kirsehir, Turkey

ABSTRACT

This study aimed to evaluate the photocatalytic activities of poly(methyl methacrylate) (PMMA)/titanium dioxide (TiO_2) nanofiber mat. TiO_2 nanoparticles in crystal phase were first prepared by sol-gel process and then PMMA/TiO_2 nanofiber mat was prepared through electrospinning. The composite (PMMA/TiO_2) nanofiber mat was compared with that of pure PMMA nanofiber mat through performing FTIR and UV-Vis spectroscopy, scanning electron microscopy, thermogravimetric analysis, weight loss and water contact angle measurements. The photocatalytic activity of PMMA/TiO_2 nanofiber mat was evaluated by investigating both the photocatalytic decomposition of a model dye, methylene blue, and photocatalytic degradation of the composite nanofiber mat in the ambient air under ultraviolet light irradiation.

ARTICLE HISTORY
Received August 2016,
Revised and Accepted
September 2016

KEYWORDS
Electrospinning; nanofiber; photocatalytic activity; photocatalytic degradation; titanium dioxide

1. Introduction

TiO_2 nanoparticles are a special type of semiconductor, which has been the focus of numerous studies due to its excellent photocatalytic and hydrophilicity properties in absorbing UV rays and its stability, cheapness and commercial availability (1). However, the powder form of TiO_2 nanoparticles is not suitable for large-scale applications. For practical application, it is more advantageous to immobilize TiO_2 nanoparticles in the polymer matrix (2). When TiO_2 nanoparticles are incorporated to a polymer matrix, all properties of the pure matrix may change depending on the properties of individual components, the shape, size, and amount of the filler, the morphology of the system (3). The main benefit of using TiO_2 nanoparticles with polymer is the improvement of matrix performance at elevated temperatures and pressures. Many researches have been performed to investigate the influence of incorporating TiO_2 nanoparticles on the performance of polymer matrices (1, 4, 5). Another benefit of using TiO_2 nanoparticles with polymer matrix is the reduction of membrane fouling. Therefore, many studies have been conducted in preparation of TiO_2 nanoparticles filled polymer composites with antifouling properties (1, 6, 7).

When TiO_2 is illuminated with UV light, the energy is greater than its band gap, promoting electrons from the valence band to the conduction band. These electrons transfer quickly to the surface of the particle and they react with oxygen and surface absorbed molecules to form superoxide and hydroxyl radicals. These active radicals are able to degrade the organic molecules by oxidizing the C-H bonds (8, 9). Regarding the photocatalytic ability of TiO_2 nanoparticles, polymer based photocatalysis UV-TiO_2 systems have been investigated to solve a variety of environmental problems such as water purification, self-cleaning material production and solid-phase photocatalytic degradation of polymer (1). The immobilization of TiO_2 nanoparticles in polymer matrix eliminates the necessity of a separation process following the water purification and prevents the problems concerning the ecotoxicity to certain extent (10). In literature, polyhydroxybutyrate/TiO_2 (2), poly (methyl methacrylate)/TiO_2 (10–12), polypyrrole/TiO_2 (13) composite systems were studied and the photocatalytic activity of the systems was determined from degradation of a model dye, methylene blue. Photodegradation experiments of methylene blue indicated that polymer/TiO_2 composite systems were found to be effective in decolorization of the model dye and they were promising in self-cleaning performance (2, 10–13).

Because of their inertness, most of polymer based materials are non-biodegradable in natural environment. They do not decompose in landfills, which causes a serious environmental problem (14). Although polymer based photocatalysis UV-TiO_2 systems have been widely researched in the remediation of wastewater pollutants, there are a few studies on the solid-phase photocatalytic degradation of TiO_2 filled polymer composite. The photocatalytic degradation of LDPE/TiO_2 (9), PS/TiO_2 (14, 15), PANI/TiO_2 (16) and PVC/TiO_2 (17, 18) was investigated. The photocatalytic degradation process of TiO_2 filled composite proceeded much faster than the simple photolysis of pure polymer (9, 14, 15, 17, 18).

Polymers in nanofiber form have an exceptionally high specific surface area, resulting in quantum efficiency, nanoscale effect of unusually high surface energy, surface reactivity, high thermal and electrical conductivity, and biodegradability. Polymer nanofibers are of considerable interest for various kinds of applications such as catalyst supports, drug delivery systems, photonics and sensors (19). Electrospinning is a unique process, creating nanofibers through an electrically charged jet of polymer solution (20). Not only pure polymer but also composite (21) and blend (22, 23) nanofibers can be prepared using electrospinning process. Electrical properties (21), surface hydrophobicity (23), thermal property (22, 23) of pure

CONTACT Ozcan Koysuren koysuren@ankara.edu.tr Department of Energy and Materials Engineering, Ankara University, Ankara, 06830, Turkey.

nanofiber can be enhanced by electrospinning of polymer matrix with functional fillers or another polymer matrix. Within this scope, TiO_2/polymer nanofiber mats, prepared by electrospinning, have been investigated as materials for the adsorption of heavy metal ions from aqueous solutions (24, 25). In addition, researchers have focused on the photocatalytic activity performance of polymer nanofiber mats functionalized with TiO_2. Photodegradation experiments of methylene blue indicated that polymer nanofiber mat containing TiO_2 nanoparticles resulted in enhanced photocatalytic activity (26–29). Also, TiO_2 included polymer nanofiber mat could be degraded by solid-phase photocatalytic degredation (30).

In this study, TiO_2 nanoparticles in crystal phase were synthesized and immobilized in PMMA nanofiber mat using via electrospinning process. Apart from the studies reported in the literature, the photocatalytic activity of PMMA/TiO_2 nanofiber mat was evaluated by investigating both the photocatalytic decomposition of methylene blue and photocatalytic degradation of the composite nanofiber mat in the ambient air under ultraviolet light irradiation.

2. Experimental

Titanium dioxide was prepared by the sol-gel process through the hydrolysis and condensation reaction of titanium isopropoxide ($Ti(OC_3H_7)_4$). 3 ml $Ti(OC_3H_7)_4$ was dissolved in 5 ml of ethyl alcohol and mixed with 2 ml of acetic acid. After stirring at room temperature for 30 min., 0.75 ml of deionized water was added to the solution. The reaction temperature was increased to 60°C when the solution was stirred. Polymeric gel structure has emerged in a short time. After drying at 80°C for 24 h, oxide powder particles were obtained. With this method, amorphous titanium dioxide was produced (Figure 1a). The calcination process was performed at 550°C to turn the produced oxide powder into the crystal phase (Figure 1b) (31).

Poly(methyl methacrylate), purchased from ABCR (Germany), was dissolved in acetone to obtain 2 wt% solution. Calcinated TiO_2 nanoparticles was mixed with 2 wt% PMMA-acetone solution to obtain 3 wt% PMMA/TiO_2 composite solution. Laboratory scale electrospinning unit (NE-100, Inovenso) was used to prepare pure PMMA and PMMA/TiO_2 nanofiber mats. Prepared solutions were filled up in a syringe and the feed rate of the solutions was maintained as 0.1 ml/hr. An electric potential difference of 40 kV was applied between the collector and the syringe tip. The distance between the collector and the tip was set as 10 cm. Pure PMMA nanofiber mat and the composite nanofiber mat were collected on the collector covered with aluminum foil.

Fourier transform infrared (FTIR) spectra of calcinated TiO_2 nanoparticles, PMMA nanofiber mat and PMMA/TiO_2 nanofiber mat were recorded with a Nicolet 380 (Thermo Scientific) spectrometer. FTIR characterization was done in the frequency range from 4000 to 400 cm^{-1} with a resolution of 2.0 cm^{-1}. The surface morphology of calcinated TiO_2 nanoparticles was examined using a scanning electron microscope (SEM: EVO LS10 ZEISS). The surface topography of pure PMMA nanofiber mat and the composite nanofiber mat were also analyzed by using SEM. The thermogravimetric analyses (TGA) of pure PMMA and PMMA/TiO_2 nanofiber mats were performed on a thermogravimetric analyzer (Setaram Labsys TGA/DTA) operating at a heating rate of 5°C/min. up to 450°C under nitrogen atmosphere. The water contact angles of pure PMMA and composite nanofiber mats were measured with a drop shape analysis system (Krüss, easydrop model) in the sessile mode at room temperature. Three different contact angle measurements were performed for each sample and average of these three test results were given with their standard deviations.

Photocatalytic activities of PMMA nanofiber mat and PMMA/TiO_2 nanofiber mat were evaluated by monitoring the degradation of the model dye, methylene blue. Pure PMMA and PMMA/TiO_2 nanofiber mat samples of size 3×3 cm^2 were immersed into 50 ml methylene blue solution with a concentration of 10 mg/L and they were held in the dark for 1 h for initialization. Then, they were exposed to UV light irradiation supplied by 8 W, 254 nm UV lamp. At specific time intervals, samples of methylene blue solution were taken out and were subjected to UV–visible spectroscopy (UV-Mini 1240 Spectrophotometer) at 665 nm to determine the dye concentration. Photocatalytic degradation of pure PMMA and PMMA/TiO_2 nanofiber mat samples (8×8 cm^2) were performed under the same UV lamp (8 W, 254 nm) in the ambient air. The degradation extent of the samples was evaluated directly by their weight loss. Each photocatalytic activity experiment used a triplicate set of samples.

3. Results and discussion

Figure 2a illustrate FTIR spectrum of TiO_2 nanoparticles in crystal phase. The weak absorption peaks between 3000–1000 cm^{-1} were assigned to C–H vibrations due to the organic

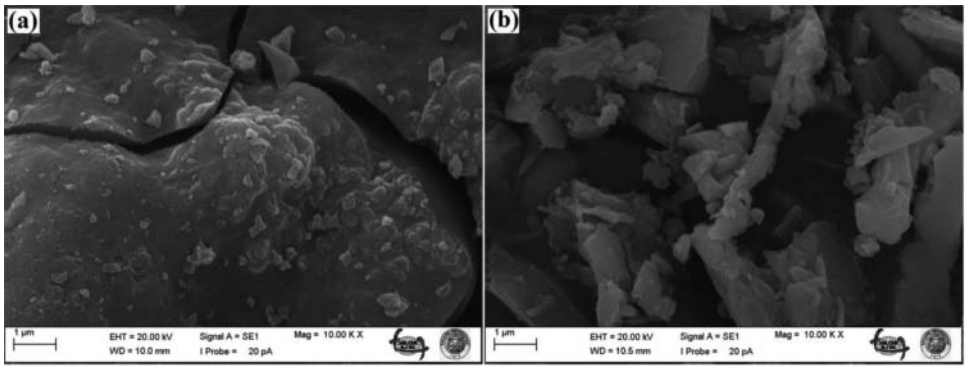

Figure 1. SEM images of (a) amorphous TiO_2 and (b) TiO_2, calcinated at 550°C.

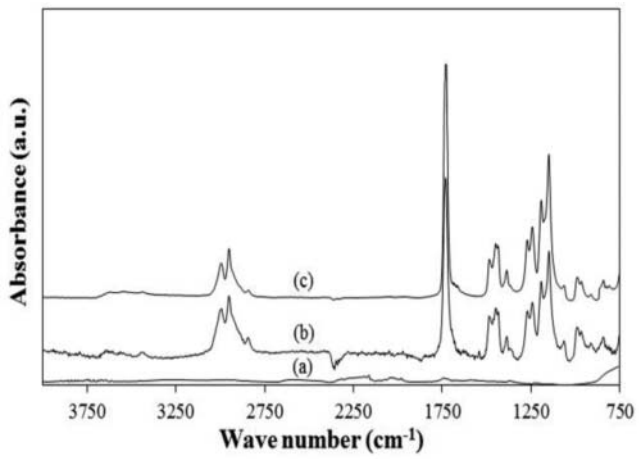

Figure 2. FTIR spectra of (a) TiO_2, calcinated at 550°C, (b) PMMA nanofiber mat and (c) PMMA/TiO_2 nanofiber mat.

residues remained in TiO_2. The source of these peaks might be the titanium isopropoxide precursor used during the synthesis of the titanium dioxide. The broad absorption peak belonging to Ti–O–Ti appears in Figure 2a in the range of 1000–750 cm^{-1} (32, 33). The characteristic peak at 1700 cm^{-1} observed in the FTIR spectra of TiO_2 nanoparticles was assigned to the stretching C=O band (34). The broad peak appearing between 3000–2700 cm^{-1} was attributed to the symmetric CH_2 stretching vibrations (35). In addition, the absorption peaks at around 2127 cm^{-1} and 1995 cm^{-1} might be arised from adsorbed CO_2 and H_2O, respectively (Figure 2a) (36). Figures 2b and 2c illustrate the FTIR spectra of both PMMA nanofiber mat and PMMA/TiO_2 nanofiber mat. There are almost no differences in the FTIR spectra of both nanofiber mat samples with its wavenumbers range from 4000 to 1000 cm^{-1}, indicating that the interaction between TiO_2 nanoparticles and PMMA matrix is physical, not chemical (15). Both nanofiber mat samples illustrate the characteristic peaks of PMMA as reported in literature (23, 37, 38). Figure 2b shows the characteristic absorptions of pure PMMA nanofiber mat at 2951, 1731, 1446, 1191 and 1149 cm^{-1}, corresponding to the stretching vibrations of C—H, C=O, CH_3, OCH_3 and C—O, respectively (23, 37, 38). In the FTIR spectrum of the composite nanofiber mat (Figure 2c), the absorption peaks in the range of 1000–750 cm^{-1} were broadened slightly due to TiO_2 nanoparticles.

The viscosity of polymer solution, used to prepare nanofiber mat through electrospinning, plays a significant role in the resultant fiber morphology by determining the extent of elongation of the solution, which will in turn have an effect on the diameter of the resultant electrospun nanofiber (20). Addition of TiO_2 nanoparticles into PMMA solution might result in an increase in the solution viscosity (39). With increased solution viscosity, the diameter of the electrospun nanofiber also increases (20). As expected, the average fiber of the composite nanofiber mat is thicker than the average fiber diameter of pure PMMA nanofiber mat (Figure 3). At the low viscosity of polymer solution, it is common to find beads along the resultant electrospun nanofiber collected on the collector. When the viscosity increases, there is a gradual change in the shape of the beads from spherical to spindle-like until a smooth fiber is obtained (20). As shown in Figure 3, less beaded fiber structures were observed on the surface of the composite nanofiber mat, which could be due to the increased viscosity of PMMA/TiO_2 solution.

Figure 4 illustrates the TGA curves of pure PMMA and PMMA/TiO_2 nanofiber mats. Both of the nanofiber mats exhibit two-step weight loss with lower residual production. The first weight loss is due to the degradation of the polymer, occuring between 270–300°C, and the second weight loss is due to the cleavage of the PMMA backbone, observed after 350°C. Pure PMMA and PMMA/TiO_2 nanofiber mats completely decomposed at around 400°C (40). According to the TGA data, TiO_2 nanoparticles slightly enhanced the thermal stability of PMMA nanofiber mat.

The water contact angle of pure PMMA nanofiber mat was 130.3° (± 3.5°), in agreement with the intrinsic hydrophobic characteristic of PMMA (23). The water contact angle was insignificantly lowered to 127.4° (± 3.1°) by introduction of TiO_2 nanoparticles. The decrease in hydrophobicity was expected since TiO_2 nanoparticles are hydrophilic in nature (25, 39). The water contact angle also depends on the surface roughness and the porosity of nanofiber mats. Enhanced surface roughness and porosity results in nanofiber mats with higher measured contact angles (23, 25). Although TiO_2 nanoparticle introduction yields rougher nanofiber mat surfaces, this effect appears to be masked by the hydrophilic character of TiO_2 nanoparticles (25).

The degradation of the model dye, methylene blue, as a function of irradiation time is illustrated in Figure 5. The

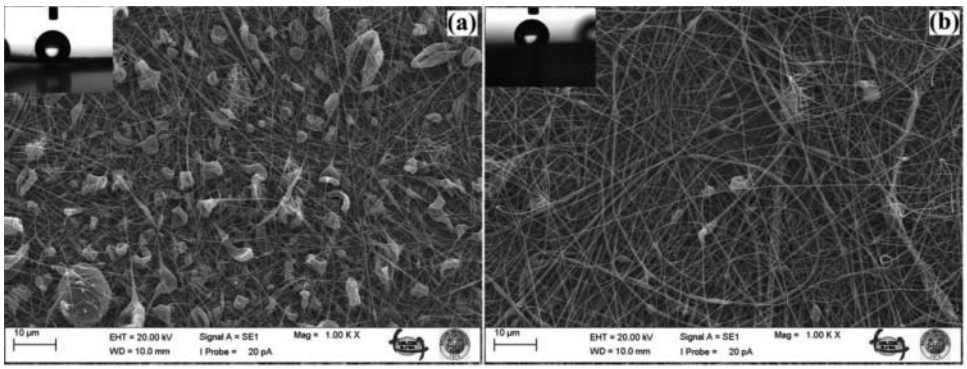

Figure 3. SEM images of (a) PMMA nanofiber mat and (b) PMMA/TiO_2 nanofiber mat.

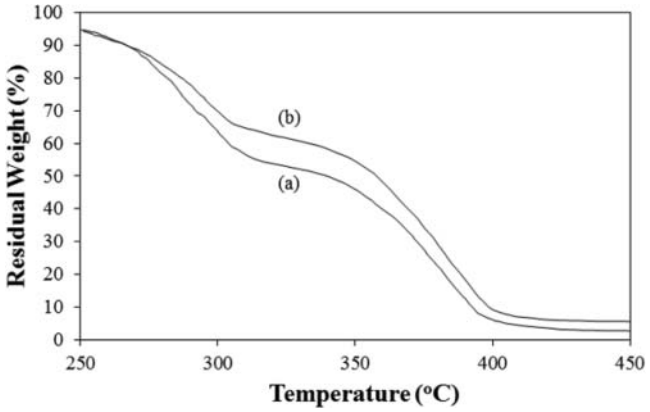

Figure 4. TGA curves of (a) PMMA nanofiber mat and (b) PMMA/TiO_2 nanofiber mat.

degradation is presented with the variation of the ratio (C/C_0) with irradiation time, where C_0 and C indicate the concentration of methylene blue solution before UV irradiation and after UV irradiation, respectively. When pure PMMA nanofiber mat was irradiated with UV, insignificant degradation of the model dye was obtained. After 180 min of irradiation, only 4% of methylene blue was degraded. On the other hand, a much better photocatalytic degradation of methylene blue occurred when TiO_2 nanoparticles were incorporated in PMMA nanofiber mat. 20% of the model dye was degraded after 180 min of UV irradiation (Figure 5). The degradation data of methylene blue obtained with pure PMMA and PMMA/TiO_2 nanofiber mats were analyzed using the pseudo-first order kinetics equation (41):

$$\ln(C_0 / C) = kt \quad (1)$$

where t is the time and k is the apparent first-order rate constant, which was obtained from the slope of the plot $\ln(C_0/C)$ vs. t (Figure 6). The discoloration rate of methylene blue for pure PMMA and PMMA/TiO_2 nanofiber mats is 0.0002 min^{-1} (R^2 = 0.987) and 0.0013 min^{-1} (R^2 = 0.992), respectively. Results showed that the composite nanofiber mat exhibited slightly higher photocatalytic activity than that of pure PMMA nanofiber mat. The reason for the limited increase in photocatalytic activity of PMMA/TiO_2 nanofiber mat might be the

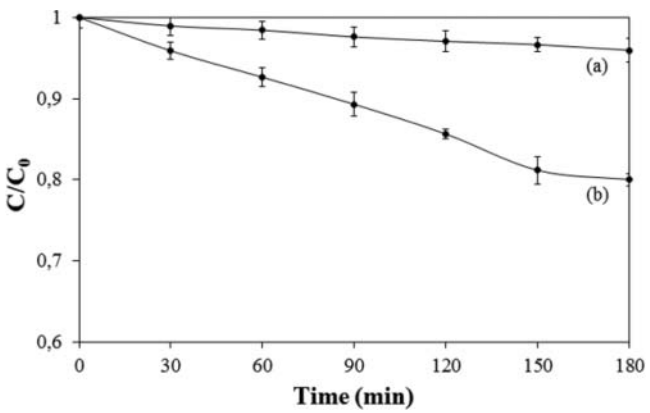

Figure 5. Photocatalytic degradation performance of methylene blue as the function of time onto (a) PMMA nanofiber mat and (b) PMMA/TiO_2 nanofiber mat.

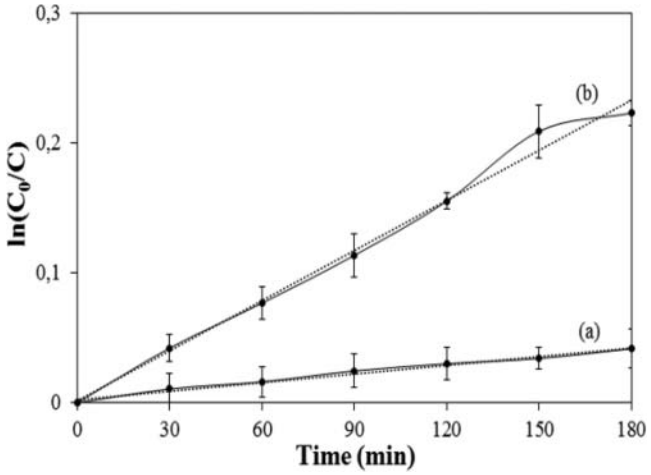

Figure 6. Photocatalytic degradation kinetics of methylene blue onto (a) PMMA nanofiber mat and (b) PMMA/TiO_2 nanofiber mat.

presence of polymer on the surface of TiO_2 nanoparticles, blocking the reactive sites of the catalyst and leading to the slower degradation rate of methylene blue (13).

Figure 7 illustrates photoinduced weight loss of both nanofiber mats in air under UV irradiation. The weight loss percent of the composite nanofiber mat reached about 4% after 192 h irradiation, while pure PMMA nanofiber mat presented only about 1% of weight loss at the same experimental condition. Photoinduced weight loss of the composite nanofiber mat might occur because of the photocatalysis reaction of TiO_2 nanoparticles and the direct photolysis reaction of PMMA (9). The weight loss percent of the composite nanofiber mat was almost 4 times higher than that of pure PMMA nanofiber mat after 192 h irradiation, indicating the dominance of the photocatalysis reaction (9). Under UV irradiation below 300 nm, the photolysis of pure PMMA nanofiber mat results in a random scission of the polymer chain backbone by a radical process and PMMA starts to degrade to lower molecular weight compounds (42). The photocatalysis reaction of TiO_2 nanoparticles is different from the photolysis reaction. When the UV light with energy higher than TiO_2 band gap is absorbed by TiO_2 nanoparticles, electron-hole pairs are generated, which can

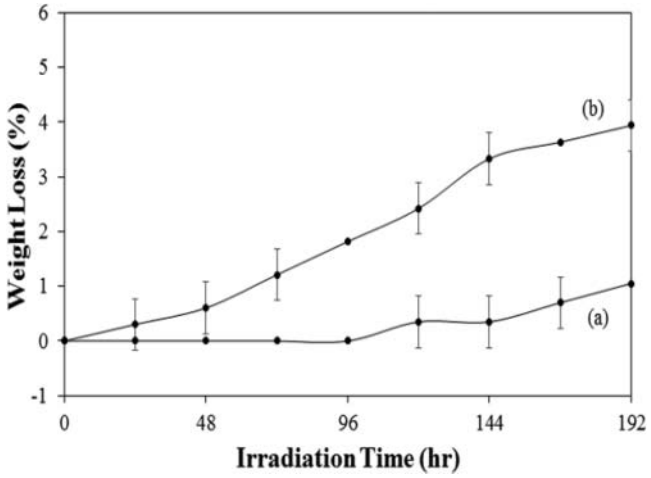

Figure 7. Weight loss of (a) PMMA nanofiber mat and (b) PMMA/TiO_2 nanofiber mat under UV irradiation as the function of time in air.

react with adsorbed oxygen and water on the surface and produce various active species such as the superoxide anion and hydroxyl radical. These active species might attack neighboring polymer chains and diffuse into the polymer matrix to continue the degradation reactions (9, 17, 30, 43, 44).

4. Conclusions

In this study, TiO_2 nanoparticles in crystal phase were synthesized and then immobilized in PMMA nanofiber mat by electrospinning process. FTIR and UV-VIS spectroscopy, SEM, TGA, weight loss and water contact angle measurements were utilized to characterize the composite nanofiber mat. The introduction of TiO_2 nanoparticles yielded thicker nanofibers with less beaded fiber structures. FTIR and TGA confirmed the presence of TiO_2 nanoparticles in the composite nanofiber mat. The loading of TiO_2 nanoparticles in PMMA nanofiber enhanced both the photocatalytic decomposition of methylene blue and photocatalytic degradation of PMMA nanofiber mat in the ambient air under ultraviolet light irradiation.

References

1. Madaeni, S. S., Ghaemi, N., Rajabi, H. In Advances in Membrane Technologies for Water Treatment: Materials, Processes and Applications, Basile, A., Cassano, A., Rastogi, N. K., Eds. Elsevier: Cambridge, UK, 3–41, 2015.
2. Yew, S. P., Tang, H. Y., Sudesh, K. (2006) Polym. Degrad. Stabil., 91 (8): 1800–1807.
3. Nielsen, L. E., Landel, R. F. Mechanical Properties of Polymer and Composites, 2nd Ed. Marcel Dekker: New York, 377–461, 1994.
4. Ebert, K., Fritsch, D., Koll, J., Tjahjawiguna, C. (2004) J. Membrane Sci., 233(1–2): 71–78.
5. Yang, Y., Wang, P. (2006) Polymer, 47(8): 2683–2688.
6. Shi, F., Ma, Y., Ma, J., Wang, P., Sun, W. (2012) J. Membrane Sci., 389: 522–531.
7. Wei, Y., Chu, H. Q., Dong, B. Z., Li, X., Xia, S. J., Qiang, Z. M. (2011) Desalination, 272(1–3): 90–97.
8. Lee, W. A., Raifailovich, M. In Inorganic Nanoparticles: Synthesis, Applications, and Perspectives, 1st Ed. Altavilla, C., Ciliberto, E., Eds. CRC Press: Boca Raton, FL, 355–367, 2011.
9. Zan, L., Fa, W., Wang, S. (2006) Environ. Sci. Technol., 40(5): 1681–1685.
10. Cantarella, M., Sanz, R., Buccheri, M. A., Ruffinoa, F., Rappazzoc, G., Scalesed, S., Impellizzeria, G., Romano, L., Privitera, V. (2016) J. Photoch. Photobio. A, 321: 1–11.
11. Yang, L., Zhou, S., Wu, L. (2015) Prog. Org. Coat., 85: 208–215.
12. Cantarella, M., Sanz, R., Buccheri, M. A., Romano, L., Privitera, V. (2016) Mat. Sci. Semicon. Proc., 42(1): 58–61.
13. Piewnuan, C., Wootthikanokkhan, J., Ngaotrakanwiwat, P., Meeyoo, V., Chiarakorn, S. (2014) Superlattice. Microst., 75: 105–117.
14. Zan, L., Tian, L., Liu, Z., Peng, Z. (2004) Appl. Catal. A-Gen., 264(2): 237–242.
15. Shang, J., Chai, M., Zhu, Y. (2003) J. Solid State Chem., 174(1): 104–110.
16. Zhang, L., Liu, P., Su, Z. (2006) Polym. Degrad. Stabil., 91(9): 2213–2219.
17. Cho, S., Choi, W. (2001) J. Photoch. Photobio. A, 143(2–3): 221–228.
18. Fa, W., Gong, C., Tian, L., Peng, T., Zan, L. (2011) J. Appl. Polym. Sci., 122(3): 1823–1828.
19. He, J. H., Liu, Y., Mo, L. F., Wan, Y. Q., Xu, L. Electrospun Nanofibres and Their Applications, iSmithers: Shropshire, UK, 1–16, 2008.
20. Ramakrishna, A., Fujihara, K., Teo, W. E., Lim, T. C., Ma, Z. An Introduction to Electrospinning and Nanofibers, World Scientific Publishing: London, 1–112, 2005.
21. Koysuren, O. (2012) J. Polym. Eng., 32(6–7): 407–413.
22. Koysuren, O., Karaman, M., Dinc, H. (2012) J. Appl. Polym. Sci., 124 (4): 2736–2741.
23. Koysuren, O., Karaman, M., Yildiz, H. B., Koysuren, H. N., Dinc, H. (2014) Int. J. Polym. Mater., 63(7): 337–341.
24. Alipour, D., Keshtkar, A. R., Moosavian, M. A. (2016) Appl. Surf. Sci., 366: 19–29.
25. Wanjale, S., Birajdar, M., Jog, J., Neppalli, R., Causin, V., Karger-Kocsis, J., Lee, J., Panzade, P. (2016) J. Colloid Interf. Sci., 469: 31–37.
26. Daels, N., Radoicic, M., Radetic, M., De Clerck, K., Van Hulle, S. W. H. (2015) Sep. Purif. Technol., 149: 488–494.
27. Mohamed, A., El-Sayed, R., Osman, T. A., Toprak, M. S., Muhammed, M., Uheida, A. (2016) Environ. Res., 145: 18–25.
28. Deniz, A. E., Celebioglu, A., Kayaci, F., Uyar, T. (2011) Mater. Chem. Phys., 129: 701–704.
29. Prahsarn, C., Klinsukhon, W., Roungpaisan, N. (2011) Mater. Lett., 65 (15–16): 2498–2501.
30. He, C. H., Gong, J. (2003) Polym. Degrad. Stabil., 81(1): 117–124.
31. Agoudjil, N., Benkacem, T. (2007) Desalination, 206(1–3): 531–537.
32. Amlouk, A., El Mir, L., Kraiem, S., Alaya, S. (2006) J. Phys. Chem. Solids, 67(7): 1464–1468.
33. Karaman, M., Sarıipek, F., Köysüren, Ö, Yıldız, H. B. (2013) Appl. Surf. Sci., 283: 993–998.
34. Baig, M. I., Ingole, P. G., Choi, W. K., Park, S. R., Kang, E. C., Lee, H. K. (2016) J. Membrane Sci., 514: 622–635.
35. Derradji, M., Ramdani, N., Zhang, T., Wang, J., Gong, L. D., Xu, X. D., Lin, Z. W., Henniche, A., Rahoma, H. K. S., Liu, W. B. (2016) Prog. Org. Coat., 90: 34–43.
36. Zapata, P. A., Rabagliati, F. M., Lieberwirth, I., Catalina, F., Corrales, T. (2014) Polym. Degrad. Stabil., 109: 106–114.
37. Yang, Y., Dan, Y. (2003) Colloid. Polym. Sci., 281(8): 794–799.
38. Yadav, J. B., Puri, R. K., Puri, V. (2007) Appl. Surf. Sci., 254(5): 1382–1388.
39. Kang, S. J., Tijing, L. D., Hwang, B. S., Jiang, Z., Kim, H. Y., Kim, C. S. (2013) Ceram. Int., 39(6): 7143–7148.
40. Abdelrazek, E. M., Hezma, A. M., El-khodary, A., Elzayat, A. M. (2016) Egypt. J. Basic Appl. Sci., 3(1): 10–15.
41. Wang, X. H., Li, J. G., Kamiyama, H., Moriyoshi, Y., Ishigaki, T. (2006) J. Phys. Chem. B, 110(13): 6804–6809.
42. Alshehry, S. D., Ismail, I. M. I. (2008) Oriental J. Chem., 24(1): 35–42.
43. Liu, G. L., Zhu, D. W., Liao, S. J., Ren, L. Y., Cui, J. Z, Zhou, W. B. (2009) J. Hazard. Mater., 172(2–3): 1424–1429.
44. Yang, C., Gong, C., Peng, T., Deng, K., Zan, L. (2010) J. Hazard. Mater., 178(1–3): 152–156.